ARTICLES
https://doi.org/10.1038/s41567-019-0594-5
nature physics

Field-tunable quantum disordered ground state in the triangular-lattice antiferromagnet $NaYbO_2$

Mitchell M. Bordelon[1], Eric Kenney[2], Chunxiao Liu[3], Tom Hogan[4], Lorenzo Posthuma[1], Marzieh Kavand[5], Yuanqi Lyu[5], Mark Sherwin[5], N. P. Butch[6], Craig Brown[6,7], M. J. Graf[2], Leon Balents[8] and Stephen D. Wilson[1*]

Antiferromagnetically coupled $S=1/2$ spins on an isotropic triangular lattice are the paradigm of frustrated quantum magnetism, but structurally ideal realizations are rare. Here, we investigate $NaYbO_2$, which hosts an ideal triangular lattice of effective $J_{eff}=1/2$ moments with no inherent site disorder. No signatures of conventional magnetic order appear down to 50 mK, strongly suggesting a quantum spin liquid ground state. We observe a two-peak specific heat and a nearly quadratic temperature dependence, in agreement with expectations for a two-dimensional Dirac spin liquid. Application of a magnetic field strongly perturbs the quantum disordered ground state and induces a clear transition into a collinear ordered state, consistent with a long-predicted up–up–down structure for a triangular-lattice XXZ Hamiltonian driven by quantum fluctuations. The observation of spin liquid signatures in zero field and quantum-induced ordering in intermediate fields in the same compound demonstrates an intrinsically quantum disordered ground state. We conclude that $NaYbO_2$ is a model, versatile platform for exploring spin liquid physics with full tunability of field and temperature.

Exotic ground states of quantum antiferromagnets are encouraged by the combination of low dimensionality, geometric frustration and inherent anisotropies. Planar triangular lattices are long-sought platforms for stabilizing them[1–7]; however, ideal manifestations that do not break crystallographic or exchange symmetries when approaching the quantum regime are rare. The organic compounds κ-$(BEDT\text{-}TTF)_2Cu_2(CN)_3$ (ref. [8]) and $EtMe_3Sb[Pd(dmit)_2]_2$ (ref. [9]) are two promising examples of triangular lattices with $S=1/2$ moments and a dynamically disordered spin ground state. However, $S=1/2$ inorganic analogues such as $Ba_3CoSb_2O_9$ (refs. [10,11]) and $NaTiO_2$ (refs. [12–14]) either order magnetically or undergo a lattice deformation when cooling. A roadblock in inorganic systems is the identification of a material with a high crystallographic symmetry, rigid structure and minimal defect mechanisms that also contains magnetic ions possessing strong quantum fluctuations. Ideally, the magnetic ions should reside at high-symmetry positions that preclude antisymmetric Dzyaloshinskii–Moriya exchange from lifting geometric frustration.

As an alternative to $S=1/2$-based compounds, rare-earth ions with ground state doublets also engender enhanced quantum fluctuations. Recent studies have shown that the spin–orbit entangled $J_{eff}=1/2$ moments of Yb^{3+} ions on a triangular lattice may exhibit a variety of nearly degenerate states[15–22]. Given the appropriate anisotropies and proximity to phase boundaries, spin liquid states are predicted to appear[22]. Recent experimental studies of one candidate material, $YbMgGaO_4$, report continuum spin dynamics and a spin-liquid-like ground state; however, chemical disorder endemic to the mixed occupancies of magnesium and gallium atoms on the same crystallographic site of this material has clouded interpretation[15–23]. Alternative models propose that the random cation distribution incites exchange disorder, facilitating the formation of a weakly bound spin glass state that experimentally resembles a spin liquid[24–26]. Fully removing this exchange disorder and accessing the physics inherent to an ideal triangular lattice of $J_{eff}=1/2$ moments remains a challenge.

The rare-earth moments in compounds of the form $NaRO_2$ (where R are rare-earth ions) are known to form an ideal triangular lattice in the α-$NaFeO_2$ ($R\text{-}3m$) structure. Previous studies suggest that they realize a large degree of magnetic frustration[27–29], and $NaYbO_2$ in particular stands out as an appealing candidate material. Specifically, the $NaYbO_2$ lattice promotes enhanced exchange through short nearest-neighbour bonds, and the ytterbium (Yb) moments occupy high-symmetry sites that forbid Dzyaloshinskii–Moriya interactions. This, combined with large crystal field splitting between the ground state and first excited doublet[20,21], renders this lattice an appealing framework.

Here, we present an investigation of the triangular lattice of Yb moments in $NaYbO_2$. Our data show that the lattice is robust and forms with fully occupied sodium and oxygen sites, minimizing potential chemical/exchange disorder. Furthermore, the structure preserves the ideal equilateral triangular lattice into the quantum regime beyond the point at which the majority of the magnetic entropy has frozen out. Zero-field susceptibility data collected down to 50 mK reveal no signatures of spin freezing or glassiness, and heat capacity data collected over the same temperature range reveal only a broad two-peak structure—a common signature of the onset of short-range correlations in materials thought to host quantum disordered ground states[30–33]. This disordered state is strongly

[1]Materials Department, University of California, Santa Barbara, Santa Barbara, CA, USA. [2]Department of Physics, Boston College, Chestnut Hill, MA, USA. [3]Department of Physics, University of California, Santa Barbara, Santa Barbara, CA, USA. [4]Quantum Design, Inc., San Diego, CA, USA. [5]Department of Physics and Center for Terahertz Science and Technology, University of California, Santa Barbara, Santa Barbara, CA, USA. [6]NIST Center for Neutron Research, National Institute of Standards and Technology, Gaithersburg, MD, USA. [7]Department of Chemical and Biomolecular Engineering, University of Delaware, Newark, DE, USA. [8]Kavli Institute for Theoretical Physics, University of California, Santa Barbara, Santa Barbara, CA, USA. *e-mail: stephendwilson@ucsb.edu

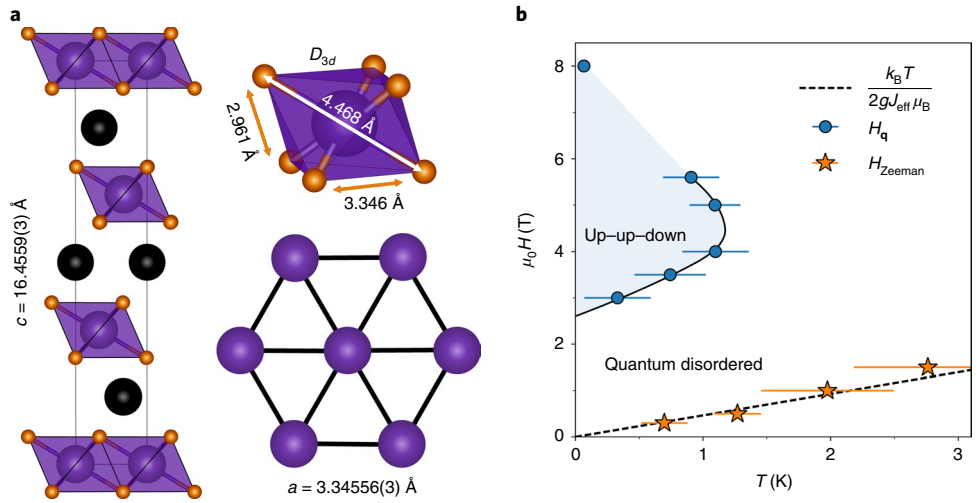

Fig. 1 | Crystal structure and magnetic (*H*, *T*) phase diagram of $NaYbO_2$. a, Refined $NaYbO_2$ structure (1.6 K, *R*3*m*) contains equilateral triangular layers of D_{3d} YbO_6 distorted octahedra separated by 3.346 Å. Sodium cations refine to full occupation, creating a uniform chemical environment surrounding the triangular layers. Purple spheres, Yb atoms; black spheres, Na atoms; brown spheres, O atoms. **b**, Low-temperature phase boundary between quantum disordered and antiferromagnetic ordered states in $NaYbO_2$, plotted as a function of field and temperature, extracted from a.c. susceptibility and neutron-scattering experiments. The dashed line denotes the boundary of Zeeman-driven quenching of a minority fraction of free Yb moments under field, above which free moments are quenched. These free moments coexist with a quantum disordered ground state. Values in parentheses and error bars indicate one standard deviation. k_B is the Boltzmann constant, $H\mathbf{q}$ denotes the onset temperature of the up–up–down ordered state and H_{Zeeman} denotes the suppression in magnetic susceptibility observed due to the quenching of a small fraction of free Yb moments.

perturbed via the application of a magnetic field that induces antiferromagnetic order consistent with an up–up–down plateau state for the triangular lattice and reflects an underlying XXZ Hamiltonian with enhanced fluctuations due to interlayer frustration. Our data reveal that $NaYbO_2$ hosts an enticing quantum disordered ground state controllable via modest external fields and presents a cleanly tunable platform for exploring order to quantum disorder phase boundaries inherent to the XXZ triangular lattice.

Polycrystalline $NaYbO_2$ was synthesized and characterized via neutron powder diffraction measurements (see Methods for further synthesis and experiment details). Figure 1a shows the structure at 1.6 K, revealing *R*3*m* symmetry with fully occupied sodium and oxygen sites. The D_{3d} distorted YbO_6 octahedra and bond lengths are illustrated, and a similar YbO_6 environment in $YbMgGaO_4$ is known to generate a large 38 meV splitting between the first excited state and the ground state doublet[20,21]. A comparison of the Yb environments of the two materials is provided in Supplementary Table 2. At low temperatures, the ground state therefore behaves as an isolated $J_{eff}=1/2$ Kramers doublet. Nearest-neighbour Yb–Yb distances were refined to 3.3507(1) Å at 300 K, consistent with previous reports[27–29], and naively support enhanced exchange relative to other frustrated Yb-based compounds.

Characterizing this exchange, magnetic susceptibility (χ) and magnetization data are plotted in Figs. 2 and 3. Below 50 K, the Van Vleck contribution to the susceptibility is negligible. The data from 20 K to 100 K were modelled by Curie–Weiss fits of the form $\frac{1}{\chi-\chi_0}=\left(\frac{C}{T-\theta_{CW}}\right)^{-1}$ (where C is specific heat, T is temperature, χ_0 is the temperature-independent contribution to the susceptibility and θ_{CW} is the Curie–Weiss temperature), shown in Fig. 2a, and yield a local moment of 2.63(8) Bohr magnetons (μ_B) with an antiferromagnetic $\theta_{CW}=-10.3(8)$ K. Relative to $YbMgGaO_4$, θ_{CW} is substantially enhanced ($\theta_{CW}=-4$ K)[15,16,18,20], consistent with enhanced exchange. The local moment suggests a heightened *g*-factor, which was validated via electron paramagnetic resonance (EPR) measurements (Fig. 2a inset). A powder-averaged *g*-factor of $g_{avg}=3.03$ is implied by the local moment extracted from susceptibility data. Fits to the EPR line shape reveal anisotropic *g*-factors of $g_{ab}=3.294(8)$ and $g_c=1.726(9)$ corresponding to the triangular *a*–*b* plane and *c* axis, respectively.

Although the saturated moment for this system is expected to be approximately 1.5 μ_B per Yb ion, $M(H)$ (where M is magnetization and H is magnetic field strength) measurements collected at 2 K up to 9 T (Fig. 2b) were able to polarize Yb moments up to 1 μ_B only, consistent with notable θ_{CW} exchange. Figure 2c shows zero-field a.c. susceptibility data collected down to 50 mK. No signatures of freezing, frequency dependence or long-range order are observed. Instead, $\chi'(T)$ continues to diverge as the sample is cooled, generating an empirical frustration parameter of $\theta_{CW}/0.050\ \text{K}>200$. As we will later argue, this zero-field state is an inherently quantum disordered state dressed by a small fraction of free Yb moments that are quenched in a magnetic field.

Data on $\chi'(T)$ collected under a variety of H fields are plotted in Fig. 2d. Under small H values, the divergence in $\chi'(T)$ (the real part of the a.c. susceptibility) is suppressed and a maximum appears. The temperature of this maximum increases with field until $\mu_0 H=2$ T (where μ_0 is the permeability of free space) is reached, beyond which $\chi'(T)$ becomes nearly temperature independent. The inflection in $\chi'(T)$ increases linearly with H and is plotted in Fig. 1b. This matches the expected Zeeman splitting (ΔE) of isolated $J_{eff}=1/2$ moments, $\Delta E=2\mu_B g_{avg} J_{eff} H$, and suggests that $\chi'(T)$ at $\mu_0 H=2$ T represents the remaining majority of the correlated/bound Yb moments. As an estimate of the fraction of free spins, $\mu_0 H=0$ T data were fit to a Curie–Weiss form after removing the majority response accessed at $\mu_0 H=2$ T. Fits to a Curie–Weiss form between 1 K and 4 K (Fig. 2d) are described by a model of 14.4(6)% free spins with a full moment of 2.63 μ_B and $\theta_{CW}=-0.45(4)$ K. In addition, 2 K $M(H)$ data plotted in Supplementary Fig. 2d were fit to a two-component model of Brillouin-like free spins and exchange-field-bound moments, which yielded a free spin fraction of approximately 7%. These fits roughly parametrize the limits of a free spin fraction in the material and suggest that free spins coexist within a quantum disordered ground state.

At higher fields, the nearly temperature-independent $\chi'(T)$ at 2 T evolves into an ordered state. Isothermal $\chi'(H)$ data at 330 mK

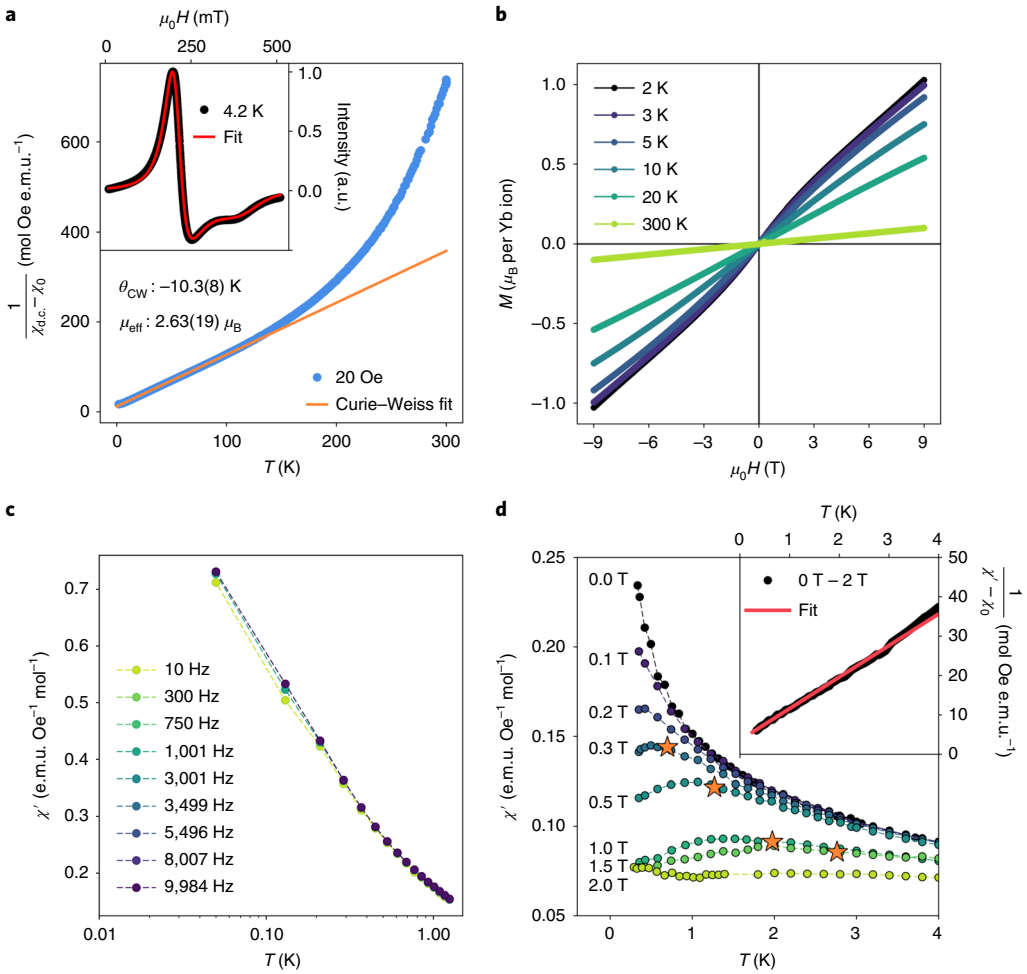

Fig. 2 | Low-field magnetization and magnetic susceptibility data. a, Low-temperature Curie–Weiss fit to the constant field magnetic susceptibility $\chi_{d.c.}$ in a temperature range free from Van Vleck contributions from high-energy crystal field doublets (where the majority of trivalent Yb ions are in the $J_{eff}=1/2$ ground state). A large mean-field interaction strength of −10.3(8) K with an effective local moment, μ_{eff}, of 2.63(19) μ_B is fit with a temperature-independent $\chi_0=0.0053(3)$ e.m.u. mol^{-1} background term. Inset: EPR data collected at 4.2 K fit to anisotropic g-factors of $g_{ab}=3.294(8)$ and $g_c=1.726(9)$. **b**, Isothermal magnetization versus field data reaching only 67% of the expected 1.5 μ_B per Yb ion polarized moment under $\mu_0 H=9$ T. **c**, Temperature and frequency dependence of a.c. magnetic susceptibility $\chi'(T)$ from 50 mK to 4 K under zero field. **d**, $\chi'(T)$ data collected under applied magnetic fields. A minority fraction of free Yb moments are quenched at low temperatures and high fields, resulting in a peak in $\chi'(T)$, and the downward inflection parameterizing this Zeeman splitting is denoted by orange stars. Inset shows field-subtracted 0 T − 2 T $\chi'(T)$ data between 1 K and 3 K and a Curie–Weiss fit quantifying the fraction of free Yb moments in the system, as described in the text. Values in parentheses and error bars indicate one standard deviation. a.u., arbitrary units.

plotted in Fig. 3a show an increase in the susceptibility as a phase boundary is traversed at 3 T, followed by nearly total suppression of $\chi'(H)$ at 5 T. For $\mu_0 H>5$ T, $\chi'(H)$ begins to recover, suggesting a higher-field phase boundary—one marking the quenching of the ordered state as spins are further polarized toward a quantum paramagnetic phase. Data collected across the ordered regime are plotted in Fig. 3b and show a sharp transition below 1 K at $\mu_0 H=4$ T. The probable origin of the enhancement in $\chi'(T)$ when entering the ordered state at 3 T is the proximity of the quantum critical point associated with the nearby 0 K phase boundary. These quantum fluctuations are suppressed when crossing the finite-temperature phase boundaries away from this point.

To further characterize $NaYbO_2$, heat capacity measurements were performed. Figure 3c shows the zero-field $C(T)$ of both $NaYbO_2$ and a non-magnetic comparator, $NaLuO_2$, plotted from 80 mK to 40 K. Consistent with susceptibility data, no sharp anomaly indicative of the onset of long-range order is observed in $NaYbO_2$. Instead, a broad feature comprising two peaks is apparent—one peak centred near 1 K and the other near 2.5 K. Two peaks in $C(T)$ are predicted in a number of theoretical models for both triangular[34,35] and kagome-based[36,37] Heisenberg lattices where a quantum spin liquid state appears. Integrating the magnetic entropy, $\Delta S_M(T)$, with the lattice contribution subtracted yields an entropy reaching 95% of $R\ln(2)$ where R is the ideal gas constant and is consistent with the nominal $J_{eff}=1/2$ magnetic doublet of $NaYbO_2$.

When applying a magnetic field, data in Fig. 3d show that the 2.5 K peak in specific heat as a function of temperature, $C_p(T)$, where pressure (p) is constant, shifts upward in temperature, similar to other frustrated magnets; however, under 5 T, a sharp anomaly appears near 1 K and is coincident with the downturn in $\chi'(T)$ at this field. Under 9 T, this sharp peak broadens and shifts lower in temperature as the system is driven into the disordered state. Integrated under 5 T, the magnetic entropy matches that of 0 T, and the lowest-temperature $C_p(T)$ is strongly suppressed once order is generated. This is consistent with the suppression of low-energy spin fluctuations when entering the ordered state, which return

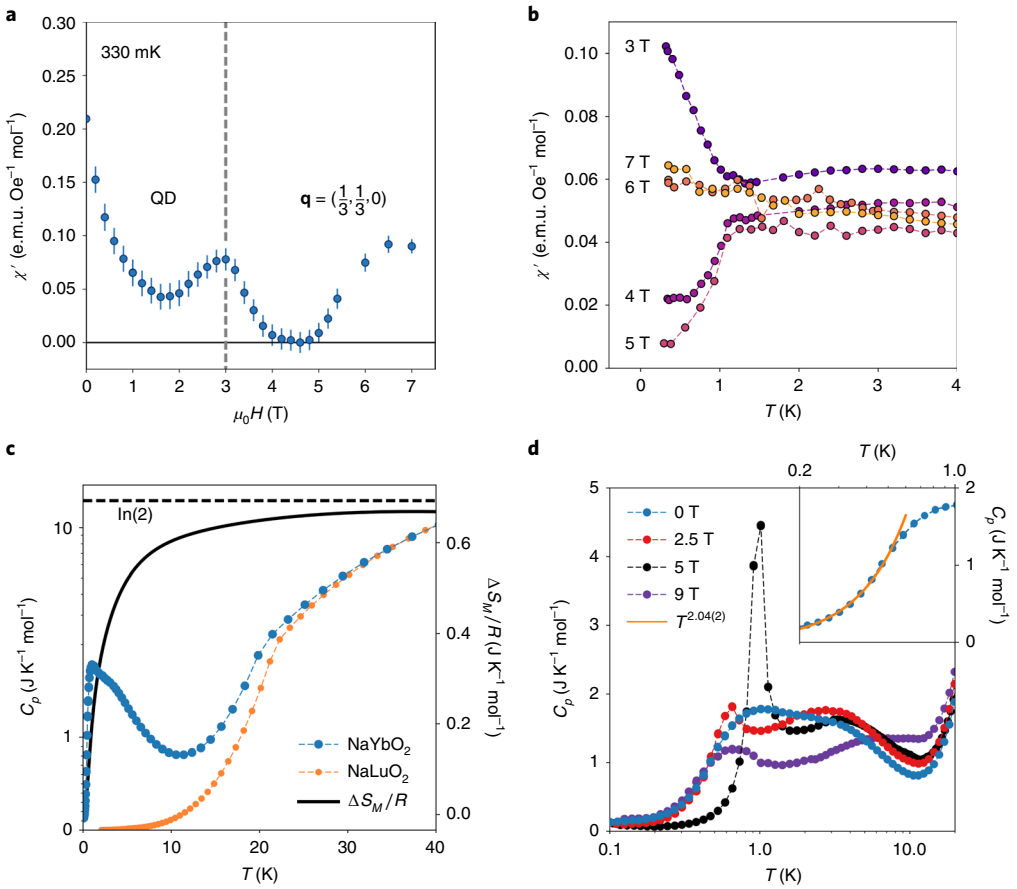

Fig. 3 | High-field magnetic susceptibility and heat capacity data. a, $\chi'(H)$ data collected at 330 mK showing the phase boundary (dashed line) between the quantum disordered (QD) ground state and magnetically ordered $\mathbf{q}=(1/3,1/3,0)$ state near 3 T. A second transition back into the quantum disordered state or a quantum paramagnetic phase begins at higher fields. **b**, $\chi'(T)$ data collected under a series of magnetic fields that traverse the ordered state; 4 T and 5 T $\chi'(T)$ data illustrate the onset of the ordered phase below 1 K, while 6 T and 7 T data suggest partial re-entry into a disordered magnetic state. **c**, Specific heat of $NaYbO_2$ measured down to 80 mK under zero field and overplotted with the non-magnetic $NaLuO_2$ analogue. The resulting magnetic entropy ΔS_M approaches 95% of $R\ln(2)$. **d**, Values of $C_p(T)$ under varying magnetic fields. The lower peak centred around 1 K develops a sharp anomaly at 5 T, indicative of the phase transition into the $\mathbf{q}=(1/3,1/3,0)$ state that is suppressed by 9 T. The inset shows the low-temperature portion of the 0 T $C_p(T)$ data fit to a power law. The resulting fit to $T^{2.04}$ is shown as a solid yellow line through the data. Error bars denote one standard deviation of the data.

when the high-field quantum paramagnetic phase is approached. Determining the precise form of the zero-field $C_p(T)$ is complicated by a nuclear Schottky feature that dominates below 100 mK (Supplementary Fig. 2c); however, attempts to do so away from this feature yield $C(T)\propto T^2$, as shown in the inset of Fig. 3d.

Low-temperature neutron-scattering measurements were also performed. Figure 4a shows temperature-subtracted (330 mK − 1.5 K) diffraction data and the absence of zero-field magnetic order. Field-subtracted data at 450 mK plotted in Fig. 4b reveal that under 5 T, new superlattice reflections appear at the momentum transfers $\mathbf{Q}=(1/3,1/3,0)$, $(1/3,1/3,1)$ and $(1/3,1/3,3)$. Given the symmetry constraints of the $R3m$ structure, these either represent a 120° non-collinear spin structure or an up–up–down pattern of spin order. The absence of a reflection at $\mathbf{Q}=(1/3,1/3,2)$ suggests that the field-induced order is collinear. Additionally, magnetic intensity appears at the $\mathbf{Q}=(0,0,3)$ position, consistent with the two-$\mathbf{q}$ or two-propagation vector structure ($\mathbf{q}=(1/3,1/3,0)+\mathbf{q}=(0,0,0)$) expected for the equal-moment up–up–down state[38]. The best fit to this model is shown in Fig. 4c, where spins refine to be oriented nearly parallel to the $(1,-1,-1)$ direction with an ordered moment of $1.36\pm0.1\,\mu_B$. This value is less than the $1.5\,\mu_B$ expected, probably due to the presence of a minority fraction of free moments as well as the influence of remnant fluctuations in the ordered state. Magnetic peaks are resolution-limited with a minimum spin–spin correlation length $\xi_{min}=450$ Å. Further data collected at 67 mK determine the low-temperature, magnetic field phase boundaries (Supplementary Fig. 4b).

Inelastic scattering data plotted in Fig. 4d,e reveal a renormalization of the low-energy spin dynamics when transitioning from the quantum disordered state into the up–up–down phase. The zero-field data show a diffuse spectrum of excitations centred around the (1/3, 1/3, 0) wave vector, and when applying a 5 T field, much of this spectral weight is shifted into the elastic channel and a nearly flat band of excitations centred at 1 meV. Powder-averaged linear spin wave calculations assuming a purely two-dimensional triangular lattice in a 5 T magnetic field reproduce this flat feature, and the simulated dynamic structure factor $S(Q, E)$ is plotted in Fig. 4f. This simulation was generated using nearest-neighbour coupling with a nearly Heisenberg Hamiltonian with a slight easy-plane anisotropy, $J_z=0.45$ and $J_{xy}=0.51$ meV. The subtle downturn at low $\mathbf{Q}$ of the 1 meV band requires easy-plane anisotropy, as discussed in the Supplementary Information.

We now discuss the implications of our results. The similar YbO_6 octahedra of $NaYbO_2$ and $YbMgGaO_4$ intimate that the local crystal fields and in-plane exchange couplings between Yb ions are comparable; however, the main distinction between the two systems

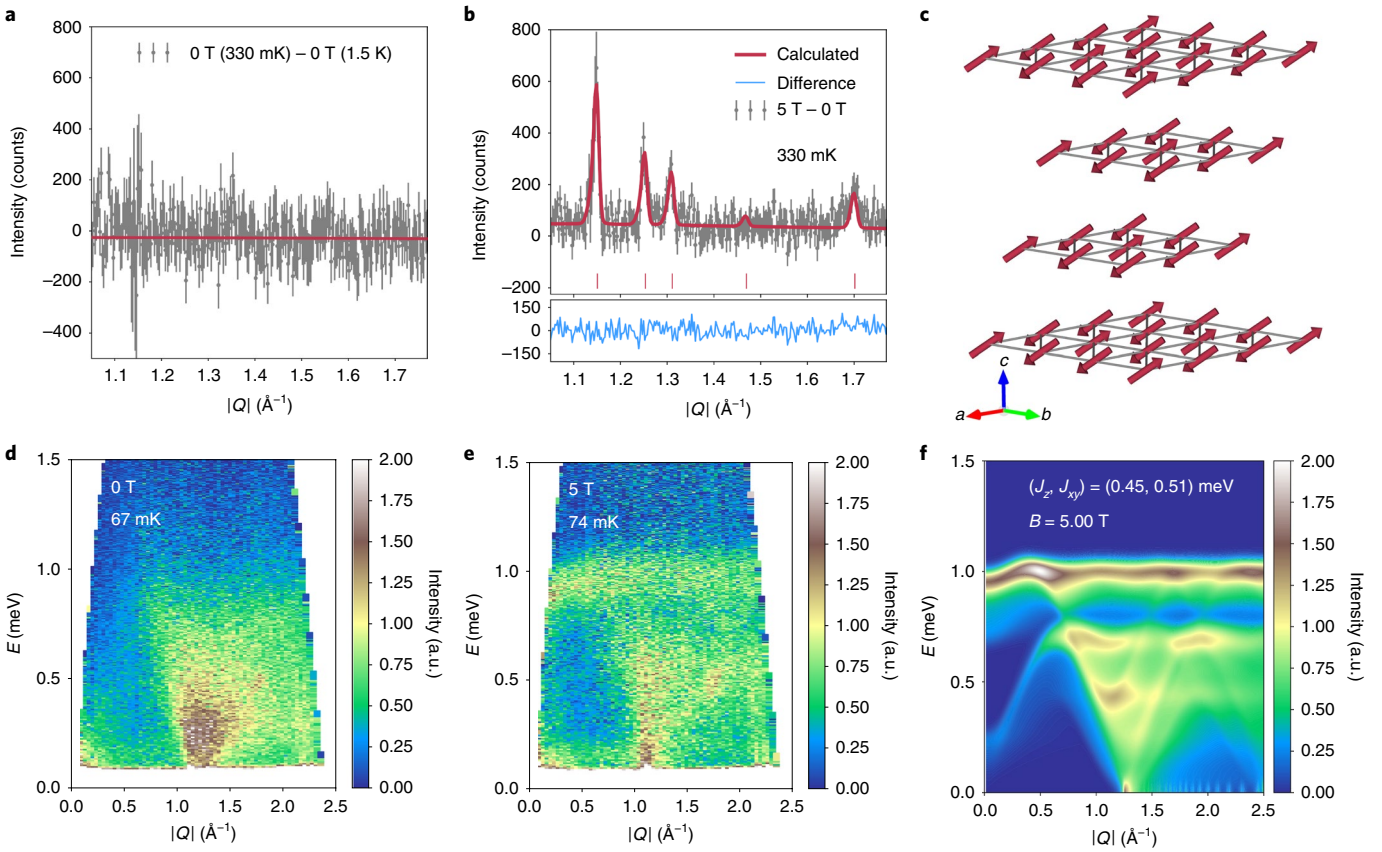

Fig. 4 | Neutron diffraction and inelastic neutron-scattering data. a, Temperature-subtracted neutron powder diffraction data (330 mK − 1.5 K) collected under 0 T, showing the absence of low-temperature magnetic order. The red line is a constant fit to the subtracted data. **b**, Under an applied field of 5 T at 450 mK, new magnetic peaks appear at (1/3, 1/3, z) positions (z = 0, 1, 3), corresponding to an ordering wave vector of $\mathbf{q}$ = (1/3, 1/3, 0). The data were refined by analysing field-subtracted data (5 T − 0 T), which are constrained by the suppressed (1/3, 1/3, 2) reflection. **c**, The best fit to the 5 T induced magnetic state using the two-$\mathbf{q}$ structure $\mathbf{q}$ = (1/3, 1/3, 0) + $\mathbf{q}$ = (0, 0, 0) is generated by a collinear spin structure with Yb moments of 1.36(10) μ_B. The displayed structure aligns moments approximately along the <1, −1, −1> direction and has six symmetrically equivalent structures generated by three-fold in-plane rotational and mirror symmetries. **d**, Inelastic neutron-scattering spectrum collected at 67 mK and 0 T. **e**, Inelastic neutron-scattering spectrum collected at 74 mK and $\mu_0 H$ = 5 T. **f**, Linear spin wave calculations showing the powder-averaged $S(Q, E)$ for a two-dimensional triangular lattice of anisotropic Yb^{3+} moments of $NaYbO_2$ in a 5 T field and three-sublattice ordering. Error bars denote one standard deviation of the data.

is the much shorter interplane distance in $NaYbO_2$. This suggests that the interlayer coupling is non-negligible, and therefore, a minimal Hamiltonian should include nearest-neighbour bonds within the planes and between neighbouring layers. Based on the structure, a symmetry analysis leads to the following exchange Hamiltonian:

$$H_{2d} = \sum_{ij} \{J_{xy}(S_i^x S_j^x + S_i^y S_j^y) + J_z S_i^z S_j^z + J_c(\hat{\mathbf{e}}_{ij} \cdot S_i)(\hat{\mathbf{e}}_{ij} \cdot S_j) + J_{cz}[(\hat{\mathbf{z}} \cdot \hat{\mathbf{e}}_{ij} \times S_i) S_j^z + (\hat{\mathbf{z}} \cdot \hat{\mathbf{e}}_{ij} \times S_j) S_i^z]\}$$

$$H' = \sum_{ij} \{J'_{xy}(S_i^x S_j^x + S_i^y S_j^y) + J'_z S_i^z S_j^z + J'_c(\hat{\mathbf{f}}_{ij} \cdot S_i)(\hat{\mathbf{f}}_{ij} \cdot S_j) + J'_{cz}[(\hat{\mathbf{f}}_{ij} \cdot S_i) S_j^z + (\hat{\mathbf{f}}_{ij} \cdot S_j) S_i^z]\}$$

The first line H_{2d} contains interactions within a triangular layer, and the second between layers. The unit vectors $\hat{\mathbf{e}}_{ij}$ are oriented along the ij bond, and $\hat{\mathbf{f}}_{ij}$ is a unit vector along the projection of the ij bond into the a–b plane. The in-plane Hamiltonian is identical to that in $YbMgGaO_4$, but is rewritten here (following Iaconis et al.[39]) in a more physically transparent 'compass model' form. The interlayer exchange H' in the second line also has a compass-like structure. We expect that this form applies to the full family of delafossite-like antiferromagnets, ARX_2 (A = alkali metal, R = rare earth and X = chalcogen ions), with dipolar Kramers doublets on the R site, sharing the space group 166.

Notably, H_{2d} contains a wide range of phase space favouring three types of classical orders: (1) three-sublattice 120° structures, (2) collinear two-sublattice stripe phases and (3) out-of-plane Ising anisotropy with up–up–down structures. Because we do not observe zero-field order, and we expect that interplane exchange is substantial, we infer that the interactions in H' should be frustrated by the in-plane order or correlations. Consideration of the coupling between layers J' uniquely singles out the three-sublattice 120° structure: to leading order, only this in-plane order allows the staggered magnetization to effectively cancel the exchange field between neighbouring planes (see Supplementary Information)[39]. This is even true to a large extent also for the anisotropic J'_c and J'_{cz} couplings.

Using this deduction that $NaYbO_2$ has 120° correlations, we expect fluctuations among many classically degenerate or nearly degenerate states to strongly suppress order. Furthermore, recent density matrix renormalization group studies of H_{2d} find that for S = 1/2 quantum spins, a spin liquid state indeed occurs in a corner of the classically 120° ordered phase space with moderate J_{cz} coupling[40]. Consequently, it is plausible that a spin liquid state

occurs in $NaYbO_2$, and if so, it is likely to be smoothly connected to the spin liquid of the two-dimensional problem. The optimal spin liquid ground state for the 2*d* model based on variational parton calculations[39] is a U(1) Dirac state with gapless fermionic spinons described theoretically as a 2+1-dimensional quantum electrodynamics (QED) conformal field theory: QED_3. The second implication of our Hamiltonian in this regime is that, on applying a magnetic field, the degeneracy is strongly lifted. This is because a large part of the zero-field cancellation is reliant on the specific 120° structure of the in-plane ground state, which is modified by the application of a magnetic field. Therefore, it is natural to expect ordering to become more robust in an applied magnetic field. The three-sublattice (1/3, 1/3, 0) wave vector is indeed germane to triangular antiferromagnets in a magnetic field, which stabilize a quantized magnetization plateau at 1/3 saturation in XXZ models[41,42].

With this in mind, we return to a discussion of the data. Theory predicts that for the 2*d* U(1) Dirac state, $C_p(T)$ is quadratic in temperature, consistent with measurements[43]. An alternative explanation of T^2 specific heat might come from the degenerate line of spiral states found by Rastelli and Tassi for the zero-field rhombohedral XXZ model[44], which has 2*d*-like spin fluctuations despite 3*d* coupling. The incommensurate long-range order of the Rastelli–Tassi spiral does not appear in our measurements; however, the field-induced Bragg peaks seen in experiment are consistent with the three-sublattice plateau states that emerge in the XXZ model in a field[41,45]. Indeed, the magnetization at 5 T, where the ordered phase is maximal, is approximately 1/3 of the expected saturation moment and corresponds to a plateau where $\chi(T) = \partial M/\partial H$ reaches zero. The best fit to neutron diffraction data further corresponds to the equal-moment two-**q** up–up–down structure of the plateau state.

The two peaks observed in the zero-field $C_p(T)$ of $NaYbO_2$ evoke a number of theoretical models of Heisenberg spins on both triangular[34,35] and kagome[36,37] lattices that predict dual entropy anomalies when cooling into spin liquid ground states. Both peaks are rarely observed experimentally, and interpretations of the nature of each peak vary with the specific model. Exact diagonalization studies of the XXZ Hamiltonian on a triangular lattice predict a high-temperature peak corresponding to the formation of trimers of doublet states (that is, short-range correlations), followed by a lower-temperature peak that marks the onset of a quantum spin singlet state[35]. Recent work exploring the $S = 1/2$ triangular lattice using tensor renormalization group techniques predicts a dual $C_p(T)$ anomaly with the lower-temperature peak signifying the onset of short-range/incipient order and the upper peak reflective of the onset of gapped low-energy chiral fluctuations[31]. The ratio of low-temperature to high-temperature peak temperatures predicted in this $S = 1/2$ model, $T_l/T_h \approx 0.36$, is consistent with those observed in $NaYbO_2$, and the $J \approx 5$ K inferred from the model is reasonably close to the θ_{CW} determined from susceptibility data.

Our data demonstrate that the nearly ideal triangular lattice of Yb ions in $NaYbO_2$ realize an unconventional quantum disordered ground state. Unlike the majority of other spin liquid candidates such as herbertsmithite ($ZnCu_3(OH)_6Cl_2$) (ref. [46]), the ground state in $NaYbO_2$ can be driven into an intermediate antiferromagnetic ordered regime in relatively weak magnetic fields. The origin of the small fraction of free spins coexisting with this ground state remains an open question; however, they are not reflective of trivial disorder, which favours the least collinear state[47]. Additionally, rather than hosting a purely two-dimensional network of spins where the two-dimensionality precludes long-range order such as in $Ba_8CoNb_6O_{24}$ (refs. [48,49]), interlayer geometric frustration is critical to the exclusion of order in $NaYbO_2$. This results in the strong perturbation that field provides to a complex interplay between interlayer frustration and the nearly degenerate ground states inherent to the XXZ triangular-lattice Hamiltonian. Due to this, $NaYbO_2$ uniquely stands able to provide considerable insight into the critical phase behaviour that manifests at the phase boundaries between the ordered and quantum disordered states in a chemically ideal frustrated triangular lattice.

Online content

Any methods, additional references, Nature Research reporting summaries, source data, statements of code and data availability and associated accession codes are available at https://doi.org/10.1038/s41567-019-0594-5.

Received: 20 December 2018; Accepted: 16 June 2019;
Published online: 29 July 2019

References

1. Anderson, P. W. Resonating valence bonds: a new kind of insulator? *Mater. Res. Bull.* **8**, 153–160 (1973).
2. Anderson, P. W. The resonating valence bond state in La_2CuO_4 and superconductivity. *Science* **235**, 1196–1198 (1987).
3. Lee, P. A. An end to the drought of quantum spin liquids. *Science* **321**, 1306–1307 (2008).
4. Balents, L. Spin liquids in frustrated magnets. *Nature* **464**, 199–208 (2010).
5. Savary, L. & Balents, L. Quantum spin liquids: a review. *Rep. Prog. Phys.* **80**, 016502 (2017).
6. Witczak-Krempa, W., Chen, G., Kim, Y. B. & Balents, L. Correlated quantum phenomena in the strong spin–orbit regime. *Annu. Rev. Condens. Matter Phys.* **5**, 57–82 (2014).
7. Zhou, Y., Kanoda, K. & Ng, T.-K. Quantum spin liquid states. *Rev. Mod. Phys.* **89**, 025003 (2017).
8. Lee, S.-S. & Lee, P. A. U(1) gauge theory of the Hubbard model: spin liquid states and possible application to κ-$(BEDT\text{-}TTF)_2Cu_2(CN)_3$. *Phys. Rev. Lett.* **95**, 036403 (2005).
9. Itou, T., Oyamada, A., Maegawa, S., Tamura, M. & Kato, R. Quantum spin liquid in the spin-1/2 triangular antiferromagnet $EtMe_3Sb[Pd(dmit)_2]_2$. *Phys. Rev. B* **77**, 104413 (2008).
10. Ma, J. et al. Static and dynamical properties of the spin-1/2 equilateral triangular-lattice antiferromagnet $Ba_3CoSb_2O_9$. *Phys. Rev. Lett.* **116**, 087201 (2016).
11. Shirata, Y., Tanaka, H., Matsuo, A. & Kindo, K. Experimental realization of a spin-1/2 triangular-lattice Heisenberg antiferromagnet. *Phys. Rev. Lett.* **108**, 057205 (2012).
12. Jackeli, G. & Ivanov, D. A. Dimer phases in quantum antiferromagnets with orbital degeneracy. *Phys. Rev. B* **76**, 132407 (2007).
13. Clarke, S. J., Fowkes, A. J., Harrison, A., Ibberson, R. M. & Rosseinsky, M. J. Synthesis, structure, and magnetic properties of $NaTiO_2$. *Chem. Mater.* **10**, 372–384 (1998).
14. McQueen, T. M. et al. Successive orbital ordering transitions in $NaVO_2$. *Phys. Rev. Lett.* **101**, 166402 (2008).
15. Li, Y. et al. Gapless quantum spin liquid ground state in the two-dimensional spin-1/2 triangular antiferromagnet $YbMgGaO_4$. *Sci. Rep.* **5**, 16419 (2015).
16. Li, Y. et al. Rare-earth triangular lattice spin liquid: a single-crystal study of $YbMgGaO_4$. *Phys. Rev. Lett.* **115**, 167203 (2015).
17. Li, Y. et al. Muon spin relaxation evidence for the U(1) quantum spin-liquid ground state in the triangular antiferromagnet $YbMgGaO_4$. *Phys. Rev. Lett.* **117**, 097201 (2016).
18. Shen, Y. et al. Evidence for a spinon Fermi surface in a triangular-lattice quantum-spin-liquid candidate. *Nature* **540**, 559–562 (2016).
19. Xu, Y. et al. Absence of magnetic thermal conductivity in the quantum spin-liquid candidate $YbMgGaO_4$. *Phys. Rev. Lett.* **117**, 267202 (2016).
20. Paddison, J. A. M. et al. Continuous excitations of the triangular-lattice quantum spin liquid $YbMgGaO_4$. *Nat. Phys.* **13**, 117–122 (2017).
21. Li, Y. et al. Crystalline electric-field randomness in the triangular lattice spin-liquid $YbMgGaO_4$. *Phys. Rev. Lett.* **118**, 107202 (2017).
22. Li, Y.-D., Wang, X. & Chen, G. Anisotropic spin model of strong spin–orbit-coupled triangular antiferromagnets. *Phys. Rev. B* **94**, 035107 (2016).
23. Li, Y.-D., Shen, Y., Li, Y., Zhao, J. & Chen, G. Effect of spin–orbit coupling on the effective-spin correlation in $YbMgGaO_4$. *Phys. Rev. B* **97**, 125105 (2018).
24. Zhu, Z., Maksimov, P. A., White, S. R. & Cheryshev, A. L. Disorder-induced mimicry of a spin liquid in $YbMgGaO_4$. *Phys. Rev. Lett.* **119**, 157201 (2017).
25. Kimchi, I., Nahum, A. & Senthil, T. Valence bonds in random quantum magnets: theory and application to $YbMgGaO_4$. *Phys. Rev. X* **8**, 031028 (2018).
26. Ma, Z. et al. Spin-glass ground state in a triangular-lattice compound $YbZnGaO_4$. *Phys. Rev. Lett.* **120**, 087201 (2018).
27. Hashimoto, Y., Wakeshima, M. & Hinatsu, Y. Magnetic properties of ternary sodium oxides $NaLnO_2$ (*Ln* = rare earths). *J. Solid State Chem.* **176**, 266–272 (2003).

28. Liu, W. et al. Rare-earth chalcogenides: a large family of triangular lattice spin liquid candidates. *Chin. Phys. Lett.* **35**, 117501 (2018).
29. Baenitz, M. et al. $NaYbS_2$: a planar spin-1/2 triangular-lattice magnet and putative spin liquid. *Phys. Rev. B* **98**, 220409(R) (2018).
30. Zeng, C. & Elser, V. Numerical studies of antiferromagnetism on a Kagomé net. *Phys. Rev. B* **42**, 8436 (1990).
31. Chen, L. et al. Two-temperature scales in the triangular-lattice Heisenberg antiferromagnet. *Phys. Rev. B* **99**, 140404(R) (2019).
32. Nambu, Y., Nakatsuji, S. & Maeno, Y. Coherent behavior and nonmagnetic impurity effects of spin disordered state in $NiGa_2S_4$. *J. Phys. Soc. Jpn* **75**, 043711 (2006).
33. Gardner, J. S., Gingras, M. J. P. & Greedan, J. E. Magnetic pyrochlore oxides. *Rev. Mod. Phys.* **82**, 53–107 (2010).
34. Wang, Y. R. Specific heat of a quantum Heisenberg model on a triangular lattice with two exchange parameters and its application to ^{3}He adsorbed on graphite. *Phys. Rev. B* **45**, 12608(R) (1992).
35. Isoda, M., Nakano, H. & Sakai, T. Specific heat and magnetic susceptibility of Ising-like anisotropic Heisenberg model on kagome lattice. *J. Phys. Soc. Jpn* **80**, 084704 (2011).
36. Elstner, N. & Young, A. P. Spin-1/2 Heisenberg antiferromagnet on the kagomé lattice: high-temperature expansion and exact-diagonalization studies. *Phys. Rev. B* **50**, 6871–6876 (1994).
37. Singh, R. R. P. & Oitmaa, J. High-temperature series expansion study of the Heisenberg antiferromagnet on the hyperkagome lattice: comparison with $Na_4Ir_3O_8$. *Phys. Rev. B* **85**, 104406 (2012).
38. Garlea, V. O. et al. Exotic magnetic field-induced spin-superstructures in a mixed honeycomb-triangular lattice system. *Phys. Rev. X* **9**, 011038 (2019).
39. Iaconis, J., Liu, C., Haláz, G. B. & Balents, L. Spin liquid versus spin orbit coupling on the triangular lattice. *SciPost Phys.* **4**, 003 (2018).
40. Zhu, Z., Maksimov, P. A., White, S. R. & Chernyshev, A. L. Topography of spin liquids on a triangular lattice. *Phys. Rev. Lett.* **120**, 207203 (2018).
41. Starykh, O. A. Unusual ordered phases of highly frustrated magnets: a review. *Rep. Prog. Phys.* **78**, 052502 (2015).
42. Chubokov, A. V. & Golosov, D. I. Quantum theory of an antiferromagnet on a triangular lattice in a magnetic field. *J. Phys.: Condens. Matter* **3**, 69–82 (1991).
43. Ran, Y., Hermele, M., Lee, P. A. & Wen, X.-G. Projected-wave-function study of the spin-1/2 Heisenberg model on the Kagomé lattice. *Phys. Rev. Lett.* **98**, 117205 (2007).
44. Rastelli, E. & Tassi, A. The rhombohedral Heisenberg antiferromagnet: infinite degeneracy of the ground state and magnetic properties of solid oxygen. *J. Phys. C: Solid State Phys.* **19**, L423–L428 (1986).
45. Ono, T. et al. Magnetization plateaux of the $S=1/2$ two-dimensional frustrated antiferromagnet Cs_2CuBr_4. *J. Phys.: Condens. Matter* **16**, S773–S778 (2004).
46. Helton, J. S. et al. Spin dynamics of the spin-1/2 kagome lattice antiferromagnet $ZnCu_3(OH)_6Cl_2$. *Phys. Rev. Lett.* **98**, 107204 (2007).
47. Maryasin, V. S. & Zhitomirsky, M. E. Triangular antiferromagnet with nonmagnetic impurities. *Phys. Rev. Lett.* **111**, 247201 (2013).
48. Rawl, R. et al. $Ba_8CoNb_6O_{24}$: a spin-1/2 triangular-lattice Heisenberg antiferromagnet in the two-dimensional limit. *Phys. Rev. B* **95**, 060412(R) (2017).
49. Cui, Y. et al. Mermin–Wagner physics, (H, T) phase diagram, and candidate quantum spin-liquid phase in the spin-1/2 triangular-lattice antiferromagnet $Ba_8CoNb_6O_{24}$. *Phys. Rev. Mater.* **2**, 044403 (2018).

Acknowledgements

This work was supported by the US Department of Energy, Office of Basic Energy Sciences, Division of Materials Sciences and Engineering under award DE-SC0017752 (S.D.W. and M.B.). M.B. acknowledges partial support by the National Science Foundation Graduate Research Fellowship Program under grant no. 1650114. Work by L.B. and C.L. was supported by the DOE, Office of Science, Basic Energy Sciences under award no. DE-FG02-08ER46524. Identification of commercial equipment does not imply recommendation or endorsement by NIST.

Author contributions

M.B., S.D.W., C.L. and L.B. wrote the manuscript. M.B. and S.D.W. analysed experiment data and planned experiments. M.J.G. and E.K. performed susceptibility measurements. M.B. and T.H. performed heat capacity and magnetization measurements. C.L. and L.B. performed theoretical analysis of the material. C.B. performed the neutron diffraction measurements, and M.B. and N.P.B. performed inelastic neutron-scattering experiments. M.S., M.K., Y.L. and M.B. performed electron spin resonance measurements. M.B. and L.P. synthesized the materials.

Competing interests

The authors declare no competing interests.

Additional information

Supplementary information is available for this paper at https://doi.org/10.1038/s41567-019-0594-5.

Reprints and permissions information is available at www.nature.com/reprints.

Correspondence and requests for materials should be addressed to S.D.W.

Publisher's note: Springer Nature remains neutral with regard to jurisdictional claims in published maps and institutional affiliations.

Methods

Sample preparation. Polycrystalline $NaYbO_2$ powder was prepared by a solid-state reaction of Yb_2O_3 (99.99%, Alfa Aesar) with Na_2CO_3 (99.997%, Alfa Aesar) in a 1/1.25 molar ratio and reacted at 1,000 °C for three days, with subsequent regrinding and reheating to 1,000 °C for another day. A slight excess of Na_2CO_3 remains in the powder and is required to prevent the formation of magnetic Yb_2O_3 impurities and stabilize the $NaYbO_2$ phase while reacting. In contrast to previous reports[27–29], attempts to remove this excess Na_2CO_3 via washing with common solvents (acidic/basic/neutral water, methanol, ethanol, isopropanol) induced $NaYbO_2$ degradation and Yb_2O_3 reformation. Therefore, the initial reaction was optimized to include minimal non-magnetic Na_2CO_3 impurities while maintaining complete reaction of Yb_2O_3 powder. All subsequent measurements accounted for the known Na_2CO_3 impurity fractions present in samples. All samples were stored in a dry, inert atmosphere and minimally exposed to atmospheric conditions before measurements. Neutron diffraction data show that the Na content of $NaYbO_2$ is stoichiometric within resolution (~1%). Although managing alkali content in many compounds can be challenging, the strong preference for Yb^{3+} aids in yielding fully occupied Na sites.

Neutron diffraction. Powder neutron diffraction data were collected on a high-resolution neutron powder diffractometer (BT-1, National Institute of Standards and Technology (NIST)). For zero-field measurements, the instrument was equipped with a cryostat capable of reaching 1.6–300 K. A 7 T vertical field cryostat with a ^{3}He insert was used to collect magnetic field data at 0 T, 5 T and 7 T between 0.33 K and 1.5 K. Samples were placed in a vanadium canister for high-temperature measurements and a copper cell for low-temperature measurements. The 300 K data were collected with neutrons of wavelengths 1.5399 Å and 2.0774 Å produced by a Cu(311) and Ge(311) monochromator, respectively. All other temperatures used neutrons of wavelength 2.0774 Å for maximum intensity. Rietveld refinement was performed with the FullProf software suite[50] and GSAS/EXPGUI programs[51,52], and fits to the data at 300 K and 1.6 K are shown in Supplementary Fig. 1. Additional inelastic neutron-scattering data were collected on a disc chopper spectrometer (NIST) in a 10 T magnetic field with a dilution insert. Incident neutrons with 5 Å wavelength were used with the medium-resolution chopper setting.

Magnetic measurements. Magnetic properties were measured using several different instruments. Isothermal d.c. magnetization up to 9 T was collected on a physical property measurement system (PPMS, Quantum Design) with a vibrating sample magnetometer insert, and low-field d.c. magnetic susceptibility from 2 K to 300 K was obtained on a magnetic property measurement system (MPMS3, Quantum Design). Isothermal a.c. susceptibility in applied fields up to 7 T and temperature-dependent a.c. magnetic susceptibility were measured on an a.c. susceptometer at 711.4 Hz with a 0.1 Oe (7.96 A m^{-1}) drive field and a ^{3}He insert capable of cooling to 330 mK. All fields collected are displayed in Supplementary Fig. 1. Within our a.c. susceptibility measurements at 711.4 Hz, the sample holder's contribution is nearly linear at this range, and this frequency-dependent background was subtracted. This was confirmed via frequency sweeps of the empty holder loaded with an equivalent amount of silver paint and thermal-link wire used for the experiment. Further zero-field, frequency-dependent, a.c. susceptibility data between 10 Hz and 10 kHz and between 50 mK and 4 K were collected with the a.c. susceptibility for dilution refrigerator option on a PPMS with a 1 Oe drive field. Measurements of the empty sample holder were performed in this a.c. susceptibility for dilution refrigerator set-up at various excitation amplitudes and frequencies to quantify the total background. Trim coils were then used to cancel (null) the measured frequency-dependent background.

EPR spectra were recorded at 4.2 K with an EMXplus (Bruker) EPR spectrometer in the perpendicular operation mode. The observed resonance line shape was modelled with the EasySpin package implemented in MATLAB (ref. [53]). Broadening of the EPR line shape was observed and could be fit to a normal distribution of the out-of-plane g_c-factor (full-width at half-maximum = 0.40(7)) with no resolvable broadening in the in-plane g_{ab}-factor.

Heat capacity measurements. Specific heat measurements between 80 mK and 300 K were performed for sintered pellets of $NaYbO_2$ under zero-field conditions on a PPMS using the dilution refrigerator insert for temperatures below 1.8 K. Data under 2.5 T, 5 T, and 9 T applied fields were also collected. The magnetic portion of specific heat was determined by subtracting the non-magnetic structural analogue $NaLuO_2$ measured between 2 K and 200 K (this was zero within resolution for temperatures <2 K). Calculated entropy was determined by integrating C_{mag}/T (where C_{mag} is the magnetic contribution to the heat capacity) between 80 mK and 40 K.

Data availability

The data that support the findings of this study are available from the corresponding author upon reasonable request. Neutron data were collected on the BT-1 diffractometer and the Disk Chopper Spectrometer at the NIST Center for Neutron Research.

References

50. Rodríguez-Carvajal, J. Recent advances in magnetic structure determination by neutron powder diffraction. *Phys. B: Condens. Matter* **192**, 55–69 (1993).
51. Larson, A. C. & Von Dreele, R. B. *General Structure Analysis System (GSAS)* Report LAUR 86-748 (Los Alamos National Laboratory, 2004).
52. Toby, B. H. EXPGUI, a graphical user interface for GSAS. *J. Appl. Crystallogr.* **34**, 210–213 (2001).
53. Stoll, S. & Schweiger, A. EasySpin, a comprehensive software package for spectral simulation and analysis in EPR. *J. Magn. Reson.* **178**, 42–55 (2006).